Journal Pre-proof

Increased central auditory gain and decreased parvalbumin-positive cortical interneuron density in the *Df1/+* mouse model of schizophrenia correlate with hearing impairment

Fhatarah A. Zinnamon, Freya G. Harrison, Sandra S. Wenas, Qing Liu, Kuan Hong Wang, Jennifer F. Linden

PII: S2667-1743(22)00032-5

DOI: https://doi.org/10.1016/j.bpsgos.2022.03.007

Reference: BPSGOS 128

To appear in: *Biological Psychiatry Global Open Science*

Received Date: 16 September 2021

Revised Date: 1 March 2022

Accepted Date: 3 March 2022

Please cite this article as: Zinnamon F.A., Harrison F.G., Wenas S.S., Liu Q., Wang K.H. & Linden J.F., Increased central auditory gain and decreased parvalbumin-positive cortical interneuron density in the *Df1/+* mouse model of schizophrenia correlate with hearing impairment, *Biological Psychiatry Global Open Science* (2022), doi: https://doi.org/10.1016/j.bpsgos.2022.03.007.

This is a PDF file of an article that has undergone enhancements after acceptance, such as the addition of a cover page and metadata, and formatting for readability, but it is not yet the definitive version of record. This version will undergo additional copyediting, typesetting and review before it is published in its final form, but we are providing this version to give early visibility of the article. Please note that, during the production process, errors may be discovered which could affect the content, and all legal disclaimers that apply to the journal pertain.

© 2022 Published by Elsevier Inc. on behalf of Society of Biological Psychiatry.

Journal Pre-proof

ARCHIVAL REPORT

Increased central auditory gain and decreased parvalbumin-positive cortical interneuron density in the *Df1/+* mouse model of schizophrenia correlate with hearing impairment

Fhatarah A. Zinnamon[1,2], Freya G. Harrison[1,3], Sandra S. Wenas[1], Qing Liu[2], Kuan Hong Wang[2,4,*] and Jennifer F. Linden[1,3,*]

[1]Ear Institute, University College London, London, UK

[2]Unit on Neural Circuits and Adaptive Behaviors, Clinical and Translational Neuroscience Branch, National Institute of Mental Health, Bethesda, MD, USA

[3]Department of Neuroscience, Physiology & Pharmacology, University College London, London, UK

[4]Department of Neuroscience, Del Monte Institute for Neuroscience, University of Rochester Medical Center, Rochester, NY, USA

*Joint corresponding authors. Contact details:

Prof. Jennifer F. Linden, UCL Ear Institute, 332 Gray's Inn Road, London WC1X 8EE, UK, Tel: +44 (0)20 7679 8936, Email: j.linden@ucl.ac.uk

Prof. Kuan Hong Wang, University of Rochester Medical Center, School of Medicine and Dentistry, 601 Elmwood Ave, Box 603, Rochester, NY 14642, USA, Tel: +1 (585) 273-4043, Email: kuanhong_wang@urmc.rochester.edu

Running title: Central auditory abnormalities in *Df1/+* mice

Keywords: 22q11.2 Deletion Syndrome, diGeorge Syndrome, Velocardiofacial Syndrome, auditory cortex, parvalbumin-positive interneurons, auditory evoked potentials

Journal Pre-proof

Journal Pre-proof

ABSTRACT

Background: Hearing impairment is a risk factor for schizophrenia. Patients with 22q11.2 Deletion Syndrome (22q11.2DS) have a 25-30% risk of schizophrenia, and up to 60% also have varying degrees of hearing impairment, primarily from middle ear inflammation. The *Df1/+* mouse model of 22q11.2DS recapitulates many features of the human syndrome, including schizophrenia-relevant brain abnormalities and high inter-individual variation in hearing ability. However, the relationship between brain abnormalities and hearing impairment in *Df1/+* mice has not been examined.

Methods: We measured auditory brainstem responses (ABRs), cortical auditory evoked potentials, and/or cortical parvalbumin-positive (PV+) interneuron density in over 70 adult mice (32 *Df1/+*, 39 wild-type). We also performed longitudinal ABR measurements in an additional 20 animals (13 *Df1/+*, 7 wild-type) from 3 weeks of age.

Results: Electrophysiological markers of central auditory excitability were elevated in *Df1/+* mice. PV+ interneurons, which are implicated in schizophrenia pathology, were reduced in density in auditory cortex but not secondary motor cortex. Both auditory brain abnormalities correlated with hearing impairment, which affected approximately 60% of adult *Df1/+* mice and typically emerged before 6 weeks of age.

Conclusions: In the *Df1/+* mouse model of 22q11.2DS, abnormalities in central auditory excitability and auditory cortical PV+ immunoreactivity correlate with hearing impairment. This is the first demonstration of cortical PV+ interneuron abnormalities correlating with hearing impairment in a mouse model of either schizophrenia or middle ear inflammation.

Journal Pre-proof

Journal Pre-proof

INTRODUCTION

The multigene deletion that causes 22q11.2 Deletion Syndrome (22q11.2DS) is the strongest known cytogenetic risk factor for schizophrenia in humans (1,2). Approximately 25-30% of patients with 22q11.2DS develop schizophrenia during adolescence or adulthood (1,3,4). Notably, up to 60% of 22q11.2DS patients have hearing impairment, arising primarily from high rates of recurrent or chronic otitis media (middle ear inflammation) (5).

The *Df1*/+ mouse model of 22q11.2DS has an engineered hemizygous deletion of 1.2Mbp encompassing 18 orthologs of genes deleted in human 22q11.2DS (6). Like other mouse models of 22q11.2DS, the *Df1*/+ mouse recapitulates many phenotypic features of the human syndrome (2,6,7), including brain and behavioral anomalies that have been linked to schizophrenia in humans (8,9). *Df1*/+ mice exhibit reduced prepulse inhibition of the acoustic startle response (10), an auditory behavioral marker for schizophrenia-like abnormalities and common feature of 22q11.2DS in humans (4). Specific abnormalities in auditory thalamocortical processing have also been reported in *Df1*/+ mice, including abnormal sensitivity of auditory thalamocortical projections to antipsychotic drugs (11). However, like humans with 22q11.2DS, up to 60% of *Df1*/+ mice have hearing impairment (12), which arises from developmental defects that increase susceptibility to otitis media (13). The potential interaction between hearing impairment and auditory brain abnormalities in *Df1*/+ mice has never been systematically explored.

In humans, hearing impairment has been described as the "neglected risk factor for psychosis" (14). Hearing loss is associated with increased risk of psychosis and hallucinations, and hearing impairment in childhood elevates the risk of developing schizophrenia later in life (15). The mechanisms underlying the association between hearing impairment and schizophrenia are unknown, and could include common etiology, top-down influences (e.g., from social isolation), and/or bottom-up effects. A role for bottom-up effects is suggested by data from animal studies indicating that reductions in peripheral auditory input drive long-lasting changes in central auditory processing which can affect behavior (16–19). Even moderate

Journal Pre-proof

conductive hearing impairment, such as that caused by otitis media, can produce persistent changes in inhibitory synaptic transmission in the auditory cortex that persist after normal hearing is restored (17,18,20,21).

Here we investigated the relationship between hearing impairment and auditory brain abnormalities in the *Df1/+* mouse model of 22q11.2DS. We focused on neurophysiological and neuroanatomical markers associated with schizophrenia in humans, such as abnormalities in cortical auditory evoked potentials (22) and parvalbumin-positive (PV+) cortical interneurons (23). PV+ interneurons play a key role in maintaining excitation-inhibition balance in the cortex (24) and abnormalities in these inhibitory cells are thought to be important to the pathophysiology of schizophrenia (25). Our results reveal a significant correlation between hearing impairment in *Df1/+* mice and both electrophysiological markers of central auditory excitability and reductions in density of PV-expressing cortical interneurons. Thus, inter-individual differences in the magnitude of brain abnormalities in the *Df1/+* mouse model of 22q11.2DS can be predicted from inter-individual differences in the degree of peripheral hearing impairment.

Journal Pre-proof

Journal Pre-proof

METHODS AND MATERIALS

Animals. *Df1/+* (also known as *Df(16)1/+*) mice (6) and their wild-type (WT) littermates were maintained in standard mouse housing facilities at either University College London (UCL) or the National Institute of Mental Health (NIMH). Experiments at UCL were performed in accordance with a Home Office project license approved under the United Kingdom Animal Scientific Procedures Act of 1986. Experiments at NIMH were approved by the local Animal Care and Use Committee. See Supplementary Information for further details.

Neurophysiology. Auditory brainstem response (ABR) and cortical auditory evoked-potential (AEP) recordings were obtained from mice anaesthetised with ketamine and either medetomidine or dexmedetomidine. All testing was performed in a sound isolation booth. Auditory stimuli were presented either via an in-ear coupler (for longitudinal ABR threshold measurements) or free-field from a speaker directed at the ear under test. For ABR threshold measurements, we used click or tone stimuli presented at 0–90 dB SPL. For comparisons of ABR and AEP wave magnitudes and latencies, we used 80 dB SPL click stimuli. ABR signals were recorded differentially between subdermal electrodes placed at the vertex (+) and behind or below the ear being tested (-), with a ground electrode either near the opposite ear (ABR threshold measurements) or over the olfactory bulb (ABR/AEP comparisons). AEP signals were recorded single-ended from subdermal electrodes placed over the temporal lobe contralateral to the ear being tested, relative to a ground over the olfactory bulb. See Supplementary Information for further details.

Journal Pre-proof

Immunohistochemistry and microscopy. Coronal brain sections (50 μm thick) were either stained alternately for Nissl substance and parvalbumin (PV), or triple-stained for PV, NeuN and DAPI. Sections stained for Nissl or DAPI were viewed at 2.5x to 5x magnifications to identify auditory cortex (A1) and secondary motor cortex (M2) with reference to a mouse brain atlas (26). Single-plane images of A1 and M2 sections immunostained for PV and NeuN were then taken at 5x to 10x magnification with 720 pixels/inch

resolution, using a Zeiss Axio Scan 2 Imaging microscope. See Supplementary Information for further details.

Data analysis: ABRs and AEPs. ABR signals were bandpass-filtered in software (100–3000 Hz, 5th-order Butterworth) before averaging across trials; AEP signals were unfiltered aside from the 2.2–7500 Hz hardware filter used in data collection. The ABR threshold was identified as in previous work (12). ABR wave I amplitude was defined as the difference in signal amplitude between the moment of sound onset and the first peak of the ABR to an 80 dB SPL click. AEP P1-N1 and N1-P2 amplitudes were defined as amplitude differences between the respective AEP wave components (27): P1, maximum peak 15-30 ms after stimulus onset; N1, maximum negative deflection 25-60 ms post-onset; and P2, maximum peak 60-110 ms post-onset. Central auditory gain was defined as the amplitude of the AEP wave complex (P1-N1 or N1-P2) divided by the amplitude of ABR wave I.

Data analysis: cell counts. PV+ and NeuN+ cell counts and laminar distributions in A1 and M2 were estimated for images from both hemispheres in each mouse when possible. Immunohistochemical data from some hemispheres and animals were lost due to problems with perfusion, damage to sections, or aberrant fluorescence in images. See Table 1 for the numbers of mice and hemispheres used for comparisons shown in Results figures.

Cortical areas of interest were defined by overlaying the section image with the mouse atlas image (26) for the corresponding coronal location, using Adobe Photoshop Elements. Cell centers were marked and centroid coordinates recorded using ImageJ. For PV analysis, all immunolabelled cells in the cortical area of interest (A1 or M2) were counted. For NeuN analysis, immunolabelled cells were counted within a smaller pia-to-white-matter rectangular strip through the center of the region of interest (5% of total area). Laminar distributions of cells were estimated using custom MATLAB software, which calculated cell centroid depth along a line perpendicular to the pial surface and white matter, normalized by the pia-to-white-matter distance in each section. Laminar distributions were compared between animal groups using cell counts

Journal Pre-proof

Journal Pre-proof

binned into 5 equal-depth bins by cortical depth; similar analyses were also performed using 10 or 20 bins in depth.

Statistical methods. All data collection and analysis was conducted blind to animal genotype, except in experiments involving longitudinal ABR measurement, which involved mostly *Df1/+* mice. Separate measurements from the same animal obtained during auditory stimulation of left versus right ears were treated as independent measurements for some data analyses, since hearing impairment in *Df1/+* mice frequently affected only one ear. Notably, the distribution of ABR thresholds for *Df1/+* ears was bimodal rather than Gaussian (i.e., normal thresholds in some *Df1/+* ears, significant hearing impairment in others). Therefore, for comparisons involving ABR threshold measurements (Figures 1–2, 7, S3), we used non-parametric tests (Wilcoxon rank-sum or signed-rank tests for differences in medians of two unpaired or paired samples; Spearman's rank correlation tests). Distributions of evoked-potential amplitudes and cell density were reasonably well approximated by Gaussian distributions. Therefore, for comparisons involving these measurements (Figures 4–6, S1–S2, S4), we used parametric tests (unpaired or paired t-tests for differences in means of two unpaired or paired samples; ordinary one-way ANOVA for comparisons between multiple groups, followed by Fisher's LSD post-hoc tests where group differences were significant). All statistical tests were two-tailed with $\alpha=0.05$.

Journal Pre-proof

Journal Pre-proof

RESULTS

Approximately 60% of adult *Df1/+* mice have hearing impairment in one or both ears

We quantified hearing sensitivity in adult *Df1/+* and WT mice aged 6.6–24.6 weeks (overall median 10.1 weeks) using the click-evoked auditory brainstem response (ABR) as in previous work (12). There was no significant difference in age between the two groups (median [95% CI]: *Df1/+* 8.3 [6.6 19.3] weeks, WT 10.4 [6.6 24.6] weeks; Wilcoxon rank-sum test, p=0.06). ABR thresholds were obtained for each ear in each mouse, except in one WT animal which died after measurement in only one ear.

Replicating previous results obtained in a cohort of older *Df1/+* and WT mice (12), we found clear evidence for hearing impairment in more than half of the *Df1/+* animals (Figure 1). Median ABR thresholds were significantly higher in *Df1/+* than WT mice (median [95% CI]: *Df1/+* 40 [30 70] dB SPL, WT 30 [30 40] dB SPL; Wilcoxon rank-sum test, p<0.0001). Elevation of ABR thresholds in *Df1/+* relative to WT mice was evident in both male and female animals, but there were no differences between genders within genotype (Figure 1A; Wilcoxon rank-sum tests, p<0.0001 between genotypes within gender, p>0.1 between genders within genotype).

Notably, there was substantial inter-ear and inter-individual variation in hearing ability among *Df1/+* animals (Figure 1B); i.e., ABR thresholds were abnormally elevated in some *Df1/+* ears but not others. Defining the upper bound of normal hearing as 2.5 SD above the mean ABR threshold for WT ears (i.e., abnormal hearing threshold: >40.88 dB SPL), we found that 46% (23/50) of *Df1/+* ears and 0% (0/51) of WT ears displayed hearing impairment. Overall, 60% (15/25) of *Df1/+* mice had either monaural or binaural hearing impairment, and monaural hearing impairment occurred most commonly in the left ear (Figure 1C). These results align both qualitatively and quantitatively with findings previously reported in *Df1/+* and WT animals tested at similar or older ages (12).

Journal Pre-proof

Hearing impairment emerges before adulthood in *Df1/+* mice

To investigate the early timecourse of hearing impairment in *Df1/+* mice, we measured click and tone ABR thresholds in mice as young as 3 weeks of age (i.e., at weaning) and conducted a longitudinal study of changes in ABR thresholds over time. This work was performed using a separate cohort of *Df1/+* and WT mice bred and tested in a different facility and country (at the National Institutes of Health, USA instead of University College London, UK).

Hearing impairment was evident in a subset of *Df1/+* mice well before adulthood. Even among mice less than 6 weeks old — i.e., before puberty in mice (28) — click ABR thresholds were elevated in *Df1/+* ears compared to WT ears (Figure 2A; median [95% CI]: *Df1/+* 35 [30 45] dB SPL vs. WT 32.5 [30 37.2] dB SPL; Wilcoxon rank-sum test, p=0.012). Moreover, early hearing impairment tended to persist in affected ears. In mice for which click ABR measurements could be obtained at both young and adult ages (<6wks and >6wks), we found significant differences in ear ABR thresholds between *Df1/+* and WT animals within both age groups, but no significant differences between ages within genotype (Figure 2B; Wilcoxon rank-sum tests, *Df1/+* vs. WT: <6wks p=0.020, >6wks p=0.0027; Wilcoxon signed-rank tests, <6wks vs. >6wks: *Df1/+* p=0.26, WT p=1).

Journal Pre-proof

Thus, hearing impairment emerged early in a subset of *Df1/+* animals and typically persisted for many weeks once it emerged. Longitudinal measurements of maximum-ear click ABR thresholds for individual mice revealed multiple examples of *Df1/+* mice with early-onset and persistent hearing impairment, along with examples of *Df1/+* mice with normal hearing across all tested ages (Figure 2C). Similar results were also obtained when measuring ABR thresholds using 8 or 16 kHz tones.

ABR wave I amplitude reductions in *Df1/+* mice with hearing impairment are not maintained in cortical AEPs

Journal Pre-proof

We wondered if auditory brain responses might differ between *Df1*/+ and WT mice, and whether any differences might be related to the hearing impairment afflicting a subset of *Df1/*+ animals. Previous studies have reported abnormalities in sound-evoked auditory thalamic and/or cortical activity in mouse models of 22q11.2DS, but have either not investigated the role of hearing impairment (11) or not observed hearing impairment in the animals tested (29).

We recorded both ABR waves and contralateral cortical auditory evoked potential (AEP) waves following presentations of loud suprathreshold (80 dB SPL) clicks at 300 ms inter-click intervals, in adult mice from the Figure 1 cohort. To assess the timing and strength of afferent input to the auditory brain, we measured the peak latency and baseline-to-peak amplitude of ABR wave I (Figure 3A), which arises from the auditory nerve. Within the AEP, we focused on wave peaks or troughs typically attributed to activity within the auditory thalamus (P1), auditory cortex (N1), and associative cortices (P2), measuring P1, N1, and P2 latency and P1-N1 and N1-P2 amplitudes (Figure 3D).

Hearing impairment, defined here as an elevation of the ABR threshold, would be expected to reduce ABR wave I amplitude for a suprathreshold click. Indeed, the amplitude of ABR wave I to an 80 dB SPL click was significantly lower in *Df1*/+ mice with hearing impairment (HI) than in either *Df1*/+ mice with no hearing impairment (NHI) or WT mice (Figure 3C and Figure 4B; one-way ANOVA, $F(2,76)=5.55$, group difference $p=0.0056$; Fisher's LSD, *Df1/*+ HI vs. WT $p=0.0094$, *Df1/*+ HI vs. *Df1/*+ NHI $p=0.0019$). However, there was no significant difference in ABR wave I amplitude between *Df1*/+ mice without hearing impairment and WT animals (Figure 3C and Figure 4B; unpaired t-test, $p=0.33$), nor between *Df1*/+ and WT mice overall (Figure 3B and Figure 4A; unpaired t-test, $p=0.66$).

More surprisingly, there were no significant differences between *Df1*/+ and WT mice in either P1-N1 or N1-P2 cortical AEP wave amplitudes, even when *Df1*/+ mice with and without hearing impairment were considered separately (Figure 3E,F and Figure 4C-F; unpaired t-test, WT vs. *Df1/*+ overall, P1-N1: $p=0.82$ and N1-P2: $p=0.22$; one-way ANOVA, WT vs. *Df1/*+ NHI vs*. Df1/*+ HI, group differences P1-N1:

Journal Pre-proof

F(2,76)=0.025, p=0.98 and N1-P2: F(2,76)=1.20, p=0.31). There were also no significant differences in latencies of ABR wave I or cortical AEP waves P1, N1 or P2 between WT and *Df1*/+ animals, either overall or when hearing impairment in *Df1*/+ mice was taken into account (Figure S1).

Thus, while ABR wave I amplitude was reduced as expected in *Df1*/+ mice with hearing impairment, there were no significant differences in the cortical AEP waves between any of the subgroups. This result suggests an increase in central auditory gain in *Df1*/+ mice with hearing impairment, as previously observed in animal models of more profound, bilateral hearing loss (e.g., (16,30)).

Central auditory gain is elevated specifically in *Df1*/+ mice with hearing impairment

To quantify central auditory gain, we compared ABR wave I amplitude to cortical AEP P1-N1 or N1-P2 amplitude recorded simultaneously over the contralateral cortical hemisphere. We used the ratios of cortical AEP P1-N1 or N1-P2 amplitude to ABR wave I amplitude as measures of central auditory gain.

Both the P1-N1 and N1-P2 gain measures revealed elevated central auditory gain specifically in *Df1*/+ mice with hearing impairment (Figure 5). When comparing *Df1/*+ mice overall with WT mice, we observed no significant differences in the ratio of either AEP P1-N1 amplitude or N1-P2 amplitude to ABR wave I amplitude (Figure 5A,C; unpaired t-test, P1-N1: p=0.36 and N1-P2: p=0.084). However, the P1-N1 gain measure was significantly higher in *Df1*/+ mice with hearing impairment than in either WT mice or *Df1*/+ mice without hearing impairment, while *Df1*/+ mice without hearing impairment were not significantly different from WT animals (Figure 5B; one-way ANOVA, F(2,76)=4.96, group difference p=0.0094; Fisher's LSD, *Df1/*+ HI vs. WT p=0.011, *Df1/*+ HI vs. *Df1/*+ NHI p=0.0037, WT vs. *Df1/*+ NHI p=0.44). Similar results were obtained for the N1-P2 gain measure (Figure 5D; one-way ANOVA, F(2,76)=7.68, group difference p=0.0009; Fisher's LSD, *Df1/*+ HI vs. WT p=0.0006, *Df1/*+ HI vs. *Df1/*+ NHI p=0.0009, WT vs. *Df1/*+ NHI p=0.79). These results suggest that central auditory abnormalities arise in some *Df1/*+ mice as a consequence of hearing impairment.

Df1/+ mice with hearing impairment have reduced density of PV+ interneurons in the auditory cortex

Changes in central auditory gain following hearing impairment have been linked with alterations in parvalbumin-positive interneuron activity in the auditory cortex (31,32), and abnormalities in PV+ interneuron networks are also a common finding in animal models of schizophrenia (see (33,34) for reviews). We wondered whether auditory cortical PV+ interneuron density might be abnormal in *Df1*/+ mice, and if so, how these abnormalities might relate to hearing impairment. To examine both PV+ cell density and density of neurons overall, we performed immunohistochemical staining for PV and NeuN (a pan-neuronal marker) in coronal brain sections through the auditory cortex (Figure 6A and Figure S2A) in adult *Df1/*+ and WT mice, most of which had also undergone ABR testing (Table 1).

PV+ cell density in the auditory cortex was significantly lower in *Df1/*+ than WT mice (Figure 6B; unpaired t-test, p=0.00030), and this difference arose primarily from abnormalities in the subset of *Df1/*+ mice with hearing impairment. In *Df1*/+ mice with hearing impairment, PV+ cell density was significantly lower than in either WT mice or *Df1*/+ mice without hearing impairment, while PV+ cell density in *Df1*/+ mice without hearing impairment did not differ from that in WT animals (Figure 6C; one-way ANOVA, F(2,43)=6.37, group difference p=0.0038; Fisher's LSD, *Df1/*+ HI vs. WT p=0.0011, *Df1/*+ HI vs. *Df1/*+ NHI p=0.026, WT vs. *Df1/*+ NHI p=0.53). In contrast, there were no significant differences in NeuN+ cell density in A1 between WT and *Df1*/+ animals with or without hearing impairment (Figure S2B,C).

Importantly, PV+ interneuron density in the auditory cortex was inversely correlated with the severity of hearing impairment in *Df1/*+ mice (Figure 7). We quantified the degree of hearing impairment in each mouse by calculating the maximum click-evoked ABR threshold across ears, and then subtracting the average of these values across WT animals. In *Df1/*+ mice, auditory cortical PV+ cell density decreased as the degree of hearing impairment increased (Figure 7; Spearman's rho=−0.42, p=0.0021). Similar trends were evident when PV+ cell density in auditory cortical hemispheres from *Df1/*+ mice were compared to left, right,

Journal Pre-proof

contralateral or ipsilateral ear ABR thresholds, with a significant negative correlation for the relationship with left ear ABR threshold in particular (Figure S3). Thus, PV+ interneuron abnormalities in the auditory cortex of *Df1/+* mice are related to the variable hearing impairment observed in these animals.

_Df1/+_ mice do not show abnormalities in PV+ or NeuN+ cell density in M2, nor changes in laminar distribution of PV+ cells in A1

Auditory cortex in mice is reciprocally connected with the secondary motor area (M2) in the frontal cortex, and neural activity in M2 is known to modulate auditory cortical processing (35,36). To find out if reductions in PV+ cell density observed in A1 of *Df1*/+ mice with hearing impairment also occurred in M2, we analyzed PV and NeuN immunostaining in coronal brain sections through frontal cortex (Figure 6D and Figure S2D).

Results suggest that reductions in PV+ cell density in *Df1/+* mice with hearing impairment may be specific to auditory cortex. PV+ cell density in M2 did not differ between WT and *Df1*/+ mice (Figure 6E; unpaired t-test, p=0.46), nor between WT mice, *Df1*/+ mice without hearing impairment, and *Df1*/+ mice with hearing impairment (Figure 6F; one-way ANOVA, F(2,56)=1.04, group difference p=0.36). There were also no significant differences between animal groups in NeuN+ cell density in M2 (Figure S2E,F).

Journal Pre-proof

Furthermore, we observed no abnormalities in laminar distribution of PV+ interneurons in A1 of *Df1/+* mice, and minimal evidence for abnormalities in M2. Comparing WT mice to *Df1/+* mice overall, we found no significant differences in the cortical depth distribution of PV+ interneurons in either A1 or M2 (Figure S4A,C). Comparing WT mice and *Df1*/+ mice with and without hearing impairment, we again found no significant differences in depth distribution of PV+ cells in A1, while a weak effect of hearing impairment was observed in M2 (Figure S4B,D). Post-hoc tests identified the significant result in M2 as arising from a reduction in PV+ cell density in *Df1/+* mice with hearing impairment, at cortical depths 0.6-0.8 of the total distance from pia to white matter. This slight alteration in M2 PV+ cell distribution in *Df1/+* mice with hearing impairment is reminiscent of aberrant laminar distributions of PV+ cells previously observed in medial

Journal Pre-proof
cortical regions of the *LgDel* mouse (37, 38). However, in M2 of *Df1/+* mice the laminar abnormalities appeared relatively weak, despite a comparatively large sample size.

Journal Pre-proof

Journal Pre-proof

DISCUSSION

Our results show that abnormalities in auditory cortical evoked potentials and PV+ interneuron density in the *Df1/+* mouse model of 22q11.2DS are related to the degree of peripheral hearing impairment in individual *Df1/+* animals. In principle, this correlation could arise from either direction of causal relationship between auditory brain abnormalities and peripheral hearing impairment, or from a common underlying cause that varies across *Df1/+* animals despite their genetic similarity.

The most plausible of the two possible causal relationships is that auditory brain abnormalities in *Df1/+* mice are caused either entirely by peripheral hearing impairment, or by an interaction between hearing impairment and other genetic vulnerabilities associated with the 22q11.2 deletion. Peripheral hearing impairment in *Df1/+* mice arises from middle ear inflammation (otitis media) triggered by developmental defects in muscles of the Eustachian tube (12,13). It is highly unlikely that auditory cortical abnormalities in *Df1/+* mice alter peripheral hearing sensitivity; even bilateral auditory cortex lesions do not affect ABR thresholds in mice (38). On the other hand, experimentally induced peripheral hearing impairment is already known to increase central auditory gain and to alter cortical excitation/inhibition balance in mice and other animals (18,31,39–41).

It is also possible that individual differences in auditory brain abnormalities and peripheral hearing impairment among *Df1/+* mice arise from a common underlying cause, such as varying levels of inflammation. Distinguishing the common-cause explanation from causal effects of hearing impairment will require further experiments in other mouse models of otitis media and in WT mice with induced hearing impairment.

Hearing impairment in mouse models of 22q11.2DS

Journal Pre-proof

Our data confirm that approximately 60% of adult *Df1*/+ mice have hearing impairment in one or both ears (12), and demonstrate for the first time that hearing impairment emerges well before adulthood in affected animals. These observations raise the possibility of developmental as well as acute effects of hearing impairment on brain function in a subset of *Df1/+* mice. Even hearing impairment that occurs only in one ear can drive plastic changes throughout the central auditory system, particularly if it occurs during development (17,20,21,42,43).

Hearing impairment in *Df1/+* mice has previously been shown to correlate ear-by-ear with otitis media (12), which is also the primary cause of hearing impairment in humans with 22q11.2DS (5). In *Df1/+* mice, susceptibility to otitis media arises from a developmental defect in a muscle affecting drainage of the middle ear through the Eustachian tube (13). This muscle defect is caused by haploinsufficiency of the gene *Tbx1* (13,44), which lies within the minimum human 22q11.2 deletion region. Thus, our present results and previous work (12,13) suggest that any mouse model of human 22q11.2DS with heterozygous deletion of *Tbx1* may be susceptible to otitis media and hearing impairment from an early age.

There are, however, some discrepant results in the literature; two previous studies that tested peripheral hearing sensitivity in mouse models of 22q11.2DS found no significant differences from WT animals (29,45). Age differences or genetic differences in the mice seem unlikely to explain the discrepant results, since hearing impairment is evident even in young *Df1/+* mice and arises from Tbx1 haploinsufficiency. Differences in the microbiological status of the mice seem a more plausible explanation, given that opportunistic pathogens in laboratory mouse facilities can increase risk of otitis media (47). Mice used in the present study were bred and maintained in standard mouse housing facilities. It is possible that the incidence of otitis media and hearing impairment in *Df1*/+ mice might be lower in super-clean facilities. Importantly, however, hearing impairment and otitis media have been found to affect a majority of human 22q11.2DS patients (5). Therefore, even if it were possible to reduce the incidence of otitis media in *Df1*/+ mice by restricting their microbiological exposure, the resulting animals would be poorer models of the human syndrome.

Journal Pre-proof

Central auditory abnormalities in mouse models of 22q11.2DS

We found that measures of central auditory gain (e.g., ratios between AEP P1-N1 or N1-P2 amplitude and ABR wave I amplitude) were significantly higher in *Df1*/+ mice with hearing impairment than in WT mice or in *Df1*/+ mice without hearing impairment. This finding is consistent with previous literature on effects of hearing impairment. Loss of peripheral auditory input drives homeostatic changes throughout the auditory brainstem, midbrain, thalamus and cortex, which typically manifest as reductions in inhibitory synaptic transmission, increased spontaneous activity, and increased gain of sound-evoked responses (16,18,21,31,49). Thus, increased central auditory gain in *Df1/*+ mice with hearing impairment could arise at multiple stages of the central auditory pathway.

Parvalbumin-positive cortical interneurons and hearing impairment

We observed a reduction in the density of PV-expressing cortical interneurons in *Df1/*+ mice, which was specific to the auditory cortex and correlated with degree of hearing impairment in individual animals.
To our knowledge, this is not only the first report of a link between hearing impairment and reduced PV+ interneuron density in an animal model of schizophrenia, but also the first indication that hearing impairment due to otitis media may influence PV+ interneuron density in the auditory cortex. Previous studies in mice have demonstrated that PV+ interneuron density and distribution in the auditory cortex can be affected by age-related changes in the auditory system (59–62), by noise-induced or pharmacologically induced sensorineural hearing loss (32,61), and by mutations that disrupt both auditory hair cell function and cortical interneuron migration (63). Our findings raise the additional possibility that conductive hearing impairment, either alone or in combination with genetic risk factors for schizophrenia, may lead to reductions in PV+ interneuron density.

Journal Pre-proof

Journal Pre-proof

Reduced PV+ cell density could arise from disrupted PV+ cell migration to cortex during embryonic development (~E13–E17), increased PV+ cell death during postnatal development (~P5–P15), and/or reduction in PV expression in cortical interneurons after development (64,65). Previous work suggests that otitis media develops soon after ear opening (at P11) in affected *Df1/+* ears (13), a finding consistent with our observation of hearing impairment in *Df1/+* mice at 3–6 weeks of age. Therefore, hearing impairment in *Df1/+* mice likely emerges after embryonic migration of PV+ cells, but might affect postnatal PV+ cell development as well as PV expression in adulthood. Further experiments are required to determine the timing of the reduction in PV+ cell density in auditory cortex.

Parvalbumin-positive cortical interneurons in mouse models of 22q11.2DS

PV+ interneurons are known to play a pivotal role in maintenance of normal cortical circuit function (57,69). Previous studies of mouse models of 22q11.2DS have reported altered laminar distribution and/or reduced density of PV+ interneurons in the medial prefrontal cortex and hippocampus (37,64–67). Abnormalities in PV+ interneurons are also a common finding in human schizophrenia, and are thought to contribute to cognitive deficits (25,70–73). Thus, auditory cortical PV+ interneuron abnormalities in mouse models of 22q11.2DS seem likely to be relevant to understanding cortical circuit dysfunction in schizophrenia — and the influence of other potential risk factors such as hearing impairment.

Implications for schizophrenia research

In humans, there is compelling evidence that hearing impairment increases the risk of psychosis and hallucinations (see (15) for a recent meta-analysis and review). Moreover, hearing impairment and/or middle ear disease in childhood is associated with elevated risk risk of developing schizophrenia in adulthood (15,76–78). The mechanisms underlying this association are unknown, but could include changes in neuronal networks driven by loss of sensory input. In individuals with genetic vulnerability to schizophrenia, including but not only 22q11.2DS patients, hearing impairment from middle ear problems

Journal Pre-proof

might be a critical "second hit" that breaks the balance of excitation and inhibition in the cortex and promotes development of hallucinations and other schizophrenia symptoms. Our results demonstrate that the *Df1/+* mouse model of 22q11.2DS is an ideal system for studying how genetic vulnerability to schizophrenia, hearing impairment, and/or interactions between these factors could produce brain abnormalities that promote psychiatric disease.

Acknowledgements:

This manuscript is a substantially revised version of a preprint previously posted on *bioRxiv (82)*. We thank Drs. T. Fitzgerald and T. Wafa for assisting FZ in conducting the auditory testing procedures at the Mouse Auditory Testing Core Facility at the National Institute on Deafness and other Communication Disorders (NIDCD), and Drs. A. Meyer and S. Mastwal for critical reading and discussion of early manuscript drafts. This work was supported by the National Institute of Mental Health Division of Intramural Research Programs ZIA MH002897 to K.H.W., Q,L. and F.Z., UCL-NIMH GPP program to F.Z., Del Monte Institute for Neuroscience at URMC to K.H.W., UKRI Medical Research Council MR/P006221/1 to J.F.L., and Action on Hearing Loss G77 to J.F.L. For the purpose of open access, the author has applied a Creative Commons Attribution (CC BY) licence to any Author Accepted Manuscript version arising.

Disclosures

The authors report no biomedical financial interests or potential conflicts of interest.

Journal Pre-proof

Journal Pre-proof

TABLE

Cell type	Area	Sample units	All WT	All *Df1/+*	WT with ABR	*Df1/+* with ABR
PV+	A1	Mice	19	19	14	14 (6 NHI, 8 HI)
		Hemispheres	32	34	22	24 (10 NHI, 14 HI)
	M2	Mice	25	21	19	16 (7 NHI, 9 HI)
		Hemispheres	43	36	31	28 (11 NHI, 17 HI)
NeuN+	A1	Mice	7	10	7	10 (4 NHI, 6 HI)
		Hemispheres	10	15	10	15 (6 NHI, 9 HI)
	M2	Mice	14	12	14	12 (6 NHI, 6 HI)
		Hemispheres	25	20	25	20 (10 NHI, 10 HI)

Table 1. Numbers of mice and brain hemispheres used for analyses of PV+ and NeuN+ cell density and laminar distribution. All mice were included in comparisons of WT and *Df1*/+ mice (Figure 6B,E; Figure S2B,E; and Figure S4A,C). Only data from mice which underwent ABR testing were included in comparisons of WT animals and *Df1*/+ mice with and without hearing impairment (Figure 6C,F; Figure S2C,F; Figure S3; and Figure S4B,D).

Journal Pre-proof

Journal Pre-proof

FIGURE LEGENDS

Figure 1. Elevated auditory brainstem response (ABR) thresholds in *Df1/+* mice.

(A) Click ABR thresholds recorded from individual ears in male and female WT (blue) and *Df1/+* (red) mice. Data points represent individual ear measurements; animals typically contributed two measurements, one for each ear. P-values indicate significant differences in Wilcoxon rank-sum tests (see text). Number of mice: 13 WT male, 13 WT female, 9 *Df1/+* male, 16 *Df1/+* female.

(B) Click ABR thresholds pooled across recordings from male and female animals. Note that the *Df1/+* ABR threshold distribution extends from the minimum to well beyond the maximum of the WT range.

(C) Relationship between left and right ear ABR thresholds in each mouse. Slight horizontal scatter added to aid visualization of overlapping data points. Dashed lines indicate the upper bound of normal hearing, defined as 2.5 SD above the mean ABR threshold for WT ears. Upper right quadrant, binaural hearing impairment; upper left and lower right quadrant, monaural hearing impairment; lower left quadrant, normal hearing. 60% (15/25) of *Df1/+* mice had either monaural or binaural hearing impairment, and 46% (23/50) of *Df1/+* ears exhibited hearing impairment. As previously observed, monaural hearing impairment in *Df1/+* mice occurred most commonly in the left ear (cf. Figure 2 in (12)).

Journal Pre-proof

Figure 2. Hearing impairment typically emerges in a subset of *Df1/+* mice before 6 weeks of age and persists into adulthood.

(A) Click ABR thresholds recorded in individual ears of WT (blue) and *Df1/+* (red) mice younger than 6 weeks old (i.e., before the typical age of sexual maturity). Data points represent individual ear ABR thresholds, averaged across any repeated measurements at ages younger than 6 weeks; each animal contributed two data points, one for each ear. Number of mice: 6 WT, 27 *Df1/+*.

(B) Click ABR thresholds measured in the same mice at 3-6 weeks (<6wks) and 6-14 weeks (>6wks) of age. Individual ear threshold estimates were averaged across repeated measurements at different time

Journal Pre-proof

points within either the <6wks age range (as in A) or the >6wks age range. Random vertical scatter (+/-3 dB SPL) added for display purposes only. P-values indicate significant differences in Wilcoxon tests (see text). Number of mice: 4 WT, 7 *Df1/+*.

(C) Maximum click-evoked ABR threshold across the two ears for each animal, shown for all measurement time points. Solid colored lines join repeated measurements from the same animal, where these could be obtained. Number of mice: 6 WT, 30 *Df1/+*. Random vertical scatter (+/-3 dB SPL) was added for display purposes only, to help separate overlapping data points.

Figure 3. Average ABR and cortical auditory evoked potential (AEP) waveforms in WT and *Df1/+* mice.

(A) Example trial-averaged ABR to an 80 dB SPL click, recorded ipsilateral to the stimulated ear in an individual WT animal. Arrows indicate baseline and peak used for measurement of wave I amplitude.

(B) Mean ABR waveforms averaged across recordings from WT mice (blue) and *Df1/+* mice (red). Error bars indicate SEM across all trial-averaged ABR recordings for each group of animals.

(C) Same as B, but with *Df1/+* ABR recordings separated into those from *Df1/+* mice without hearing impairment (green, NHI) or *Df1/+* mice with hearing impairment in at least one ear (magenta, HI).

(D) Example trial-averaged AEP to an 80 dB SPL click, recorded over auditory cortex contralateral to the stimulated ear in a WT animal. Arrows indicate P1 peak, N1 trough, and P2 peak.

(E) Mean AEP waveforms averaged across recordings from different mice; color conventions as in B. Error bars indicate SEM across all trial-averaged AEP recordings for each group of animals.

(F) Same as E, but with *Df1/+* AEP recordings separated into those from *Df1/+* mice with or without hearing impairment in at least one ear; color conventions as in C.

Ipsilateral ABR and contralateral AEP data were obtained from the same recording for each stimulated ear; however ABR waveforms in A-C represent differential signals while AEP waveforms in D-F are single-ended signals (see Materials and Methods). Each animal typically contributed two data points, one for each

Journal Pre-proof

Journal Pre-proof

ear/hemisphere combination. Number of mice: 20 WT, 20 *Df1/+* (11 *Df1/+* NHI, 9 *Df1/+* HI). Number of ABR/AEP recordings: 39 WT, 40 *Df1/+* (22 *Df1/+* NHI, 18 *Df1/+* HI).

Figure 4. Reductions in ABR wave I amplitude in *Df1/+* mice with hearing impairment are not maintained in cortical AEPs. See text for details of statistical tests.

(A) ABR wave I amplitude to an 80 dB SPL click does not differ between WT and *Df1/+* mice overall.

(B) However, wave I amplitude to an 80 dB SPL click is reduced in *Df1/+* mice with hearing impairment relative to either WT mice or *Df1/+* mice without hearing impairment, while there is no significant difference in ABR wave I amplitude between *Df1/+* mice without hearing impairment and WT mice.

(C-D) AEP P1-N1 amplitude does not differ between WT and *Df1/+* mice, either overall (C) or when *Df1/+* mice with and without hearing impairment are considered separately (D).

(E-F) No significant differences in AEP N1-P2 amplitude between WT and *Df1/+* mice, either overall (E), or when *Df1/+* mice with and without hearing loss impairment are considered separately (F).

Number of mice, number of ABR/AEP recordings, and color conventions as in Figure 2. Bars and error bars indicate mean ± SEM across recordings.

Journal Pre-proof

Figure 5. Central auditory gain is elevated in *Df1/+* mice with hearing impairment. See text for details of statistical tests.

(A) The ratio of AEP P1-N1 amplitude to ABR wave I amplitude for an 80 dB SPL click does not differ between WT mice and *Df1/+* mice overall.

(B) However, this measure of central auditory gain for the P1-N1 complex is significantly elevated in *Df1/+* mice with hearing impairment relative to either WT mice or *Df1/+* mice without hearing impairment.

(C) Same as A but for the ratio of AEP N1-P2 amplitude to ABR wave I amplitude; no difference between WT mice and *Df1/+* mice overall.

(D) Central auditory gain for the N1-P2 complex is significantly elevated in *Df1/+* mice with hearing impairment relative to either WT mice or *Df1/+* mice without hearing impairment.

Number of mice and number of ABR/AEP recordings as in Figures 2 and 3; plot conventions as in Figure 3.

Figure 6. PV+ cell density is reduced in the auditory cortex but not the motor cortex of *Df1/+* mice.

(A) Example confocal image used for cell counting. Coronal section through primary auditory cortex (A1) stained with an antibody against the inhibitory interneuron marker parvalbumin (PV). Areas outside A1 are masked in black. Scale bar: 0.1 mm.

(B) PV+ cell density in A1 was significantly reduced in *Df1/+* mice overall compared to WT mice.

(C) PV+ cell density in A1 was significantly reduced in *Df1/+* mice with hearing impairment compared to either WT mice or *Df1/+* mice without hearing impairment, but there was no significant difference between WT mice and *Df1/+* mice without hearing impairment.

(D) Example PV-immunostained coronal section used for cell counting in secondary motor cortex (M2). Areas outside M2 are masked in black. Scale bar as in A.

(E) In M2, there was no significant difference in PV+ cell density between *Df1/+* and WT mice overall.

(F) PV+ cell density in M2 also did not differ between groups when comparing WT mice, *Df1/+* mice without hearing impairment, and *Df1/+* mice with hearing impairment.

See text for details of statistical tests, and Table 1 for numbers of hemispheres (and mice) in each comparison.

Figure 7. PV+ cell density in the auditory cortex correlates inversely with hearing impairment in *Df1/+* mice.

Each data point (blue, WT; red, *Df1/+*) represents a PV+ cell density measurement from A1 in the left or right hemisphere; individual mice typically contributed two measurements, one for each hemisphere. Here, hemisphere measurements are plotted against an overall measure of hearing impairment for each animal

Journal Pre-proof

Journal Pre-proof

(x-axis), obtained by calculating the maximum click-evoked ABR threshold across ears, and then subtracting the mean of these values across WT animals only. For comparisons of PV+ cell density in each hemisphere to left, right, contralateral, and ipsilateral ear ABR thresholds, see Figure S3. Red text, Spearman's rho and p-value for correlation of PV+ cell density with hearing impairment, for *Df1/+* mice only. Solid red line, two-dimensional least-squares linear fits to the *Df1/+* data. Number of mice and number of hemispheres as in Table 1 and Figure 6.

Journal Pre-proof

REFERENCES

1. McDonald-McGinn DM, Sullivan KE, Marino B, Philip N, Swillen A, Vorstman JAS, et al. 22q11.2 deletion syndrome. Nat Rev Dis Primers. 2015 Nov 19;1:15071.
2. Paylor R, Lindsay E. Mouse models of 22q11 deletion syndrome. Biol Psychiatry. 2006 Jun 15;59(12):1172–9.
3. Schneider M, Debbané M, Bassett AS, Chow EWC, Fung WLA, van den Bree M, et al. Psychiatric disorders from childhood to adulthood in 22q11.2 deletion syndrome: results from the International Consortium on Brain and Behavior in 22q11.2 Deletion Syndrome. Am J Psychiatry. 2014 Jun;171(6):627–39.
4. Drew LJ, Crabtree GW, Markx S, Stark KL, Chaverneff F, Xu B, et al. The 22q11.2 microdeletion: fifteen years of insights into the genetic and neural complexity of psychiatric disorders. Int J Dev Neurosci. 2011 May;29(3):259–81.
5. Verheij E, Derks LSM, Stegeman I, Thomeer HGXM. Prevalence of hearing loss and clinical otologic manifestations in patients with 22q11.2 deletion syndrome: A literature review. Clin Otolaryngol. 2017 Dec;42(6):1319–28.
6. Lindsay EA, Botta A, Jurecic V, Carattini-Rivera S, Cheah YC, Rosenblatt HM, et al. Congenital heart disease in mice deficient for the DiGeorge syndrome region. Nature. 1999 Sep 23;401(6751):379–83.
7. Aggarwal VS, Liao J, Bondarev A, Schimmang T, Lewandoski M, Locker J, et al. Dissection of Tbx1 and Fgf interactions in mouse models of 22q11DS suggests functional redundancy. Hum Mol Genet. 2006 Nov 1;15(21):3219–28.
8. Hamm JP, Peterka DS, Gogos JA, Yuste R. Altered cortical ensembles in mouse models of schizophrenia. Neuron. 2017 Apr 5;94(1):153-167.e8.
9. Sigurdsson T, Stark KL, Karayiorgou M, Gogos JA, Gordon JA. Impaired hippocampal-prefrontal synchrony in a genetic mouse model of schizophrenia. Nature. 2010 Apr 1;464(7289):763–7.
10. Paylor R, McIlwain KL, McAninch R, Nellis A, Yuva-Paylor LA, Baldini A, et al. Mice deleted for the DiGeorge/velocardiofacial syndrome region show abnormal sensorimotor gating and learning and memory impairments. Hum Mol Genet. 2001 Nov 1;10(23):2645–50.
11. Chun S, Westmoreland JJ, Bayazitov IT, Eddins D, Pani AK, Smeyne RJ, et al. Specific disruption of thalamic inputs to the auditory cortex in schizophrenia models. Science. 2014 Jun 6;344(6188):1178–82.
12. Fuchs JC, Zinnamon FA, Taylor RR, Ivins S, Scambler PJ, Forge A, et al. Hearing loss in a mouse model of 22q11.2 Deletion Syndrome. PLoS ONE. 2013 Nov 14;8(11):e80104.
13. Fuchs JC, Linden JF, Baldini A, Tucker AS. A defect in early myogenesis causes Otitis media in two mouse models of 22q11.2 Deletion Syndrome. Hum Mol Genet. 2015 Apr 1;24(7):1869–82.
14. Sommer IE, Roze CM, Linszen MMJ, Somers M, van Zanten GA. Hearing loss; the neglected risk factor for psychosis. Schizophr Res. 2014 Sep;158(1–3):266–7.
15. Linszen MMJ, Brouwer RM, Heringa SM, Sommer IE. Increased risk of psychosis in patients with hearing impairment: Review and meta-analyses. Neurosci Biobehav Rev. 2016 Mar;62:1–20.
16. Chambers AR, Resnik J, Yuan Y, Whitton JP, Edge AS, Liberman MC, et al. Central Gain Restores Auditory Processing following Near-Complete Cochlear Denervation. Neuron. 2016 Feb 17;89(4):867–79.

Journal Pre-proof

Journal Pre-proof

17. Sanes DH, Kotak VC. Developmental plasticity of auditory cortical inhibitory synapses. Hear Res. 2011 Sep;279(1–2):140–8.

18. Takesian AE, Kotak VC, Sanes DH. Developmental hearing loss disrupts synaptic inhibition: implications for auditory processing. Future Neurol. 2009 May 1;4(3):331–49.

19. Yao JD, Sanes DH. Developmental deprivation-induced perceptual and cortical processing deficits in awake-behaving animals. eLife. 2018 Jun 6;7.

20. Mowery TM, Kotak VC, Sanes DH. Transient hearing loss within a critical period causes persistent changes to cellular properties in adult auditory cortex. Cereb Cortex. 2015 Aug;25(8):2083–94.

21. Takesian AE, Kotak VC, Sanes DH. Age-dependent effect of hearing loss on cortical inhibitory synapse function. J Neurophysiol. 2012 Feb;107(3):937–47.

22. Bramon E, Rabe-Hesketh S, Sham P, Murray RM, Frangou S. Meta-analysis of the P300 and P50 waveforms in schizophrenia. Schizophr Res. 2004 Oct 1;70(2–3):315–29.

23. Lewis DA, Hashimoto T, Volk DW. Cortical inhibitory neurons and schizophrenia. Nat Rev Neurosci. 2005 Apr;6(4):312–24.

24. Moore AK, Weible AP, Balmer TS, Trussell LO, Wehr M. Rapid rebalancing of excitation and inhibition by cortical circuitry. Neuron. 2018 Mar 21;97(6):1341-1355.e6.

25. Lewis DA. Inhibitory neurons in human cortical circuits: substrate for cognitive dysfunction in schizophrenia. Curr Opin Neurobiol. 2014 Jun;26:22–6.

26. Paxinos G, Franklin KBJ. Paxinos and Franklin's the Mouse Brain in Stereotaxic Coordinates. 4th ed. Academic Press; 2012.

27. Maxwell CR, Liang Y, Weightman BD, Kanes SJ, Abel T, Gur RE, et al. Effects of chronic olanzapine and haloperidol differ on the mouse N1 auditory evoked potential. Neuropsychopharmacology. 2004 Apr;29(4):739–46.

28. Dutta S, Sengupta P. Men and mice: Relating their ages. Life Sci. 2016 May 1;152:244–8.

29. Didriksen M, Fejgin K, Nilsson SRO, Birknow MR, Grayton HM, Larsen PH, et al. Persistent gating deficit and increased sensitivity to NMDA receptor antagonism after puberty in a new mouse model of the human 22q11.2 microdeletion syndrome: a study in male mice. J Psychiatry Neurosci. 2017;42(1):48–58.

30. Teichert M, Liebmann L, Hübner CA, Bolz J. Homeostatic plasticity and synaptic scaling in the adult mouse auditory cortex. Sci Rep. 2017 Dec 12;7(1):17423.

31. Resnik J, Polley DB. Cochlear neural degeneration disrupts hearing in background noise by increasing auditory cortex internal noise. Neuron. 2021 Mar 17;109(6):984-996.e4.

32. Resnik J, Polley DB. Fast-spiking GABA circuit dynamics in the auditory cortex predict recovery of sensory processing following peripheral nerve damage. eLife. 2017 Mar 21;6.

33. Selten M, van Bokhoven H, Nadif Kasri N. Inhibitory control of the excitatory/inhibitory balance in psychiatric disorders. [version 1; peer review: 2 approved]. F1000Res. 2018 Jan 8;7:23.

34. Lewis DA, Curley AA, Glausier JR, Volk DW. Cortical parvalbumin interneurons and cognitive dysfunction in schizophrenia. Trends Neurosci. 2012 Jan;35(1):57–67.

35. Nelson A, Schneider DM, Takatoh J, Sakurai K, Wang F, Mooney R. A circuit for motor cortical modulation of auditory cortical activity. J Neurosci. 2013 Sep 4;33(36):14342–53.

Journal Pre-proof

Journal Pre-proof

36. Schneider DM, Nelson A, Mooney R. A synaptic and circuit basis for corollary discharge in the auditory cortex. Nature. 2014 Sep 11;513(7517):189–94.

37. Meechan DW, Tucker ES, Maynard TM, LaMantia A-S. Diminished dosage of 22q11 genes disrupts neurogenesis and cortical development in a mouse model of 22q11 deletion/DiGeorge syndrome. Proc Natl Acad Sci USA. 2009 Sep 22;106(38):16434–45.

38. Hunter KP, Willott JF. Effects of bilateral lesions of auditory cortex in mice on the acoustic startle response. Physiol Behav. 1993 Dec;54(6):1133–9.

39. Kotak VC, Fujisawa S, Lee FA, Karthikeyan O, Aoki C, Sanes DH. Hearing loss raises excitability in the auditory cortex. J Neurosci. 2005 Apr 13;25(15):3908–18.

40. Kotak VC, Takesian AE, Sanes DH. Hearing loss prevents the maturation of GABAergic transmission in the auditory cortex. Cereb Cortex. 2008 Sep;18(9):2098–108.

41. Persic D, Thomas ME, Pelekanos V, Ryugo DK, Takesian AE, Krumbholz K, et al. Regulation of auditory plasticity during critical periods and following hearing loss. Hear Res. 2020 Nov;397:107976.

42. Popescu MV, Polley DB. Monaural deprivation disrupts development of binaural selectivity in auditory midbrain and cortex. Neuron. 2010 Mar 11;65(5):718–31.

43. Keating P, Dahmen JC, King AJ. Complementary adaptive processes contribute to the developmental plasticity of spatial hearing. Nat Neurosci. 2015 Feb;18(2):185–7.

44. Liao J, Kochilas L, Nowotschin S, Arnold JS, Aggarwal VS, Epstein JA, et al. Full spectrum of malformations in velo-cardio-facial syndrome/DiGeorge syndrome mouse models by altering Tbx1 dosage. Hum Mol Genet. 2004 Aug 1;13(15):1577–85.

45. Paylor R, Glaser B, Mupo A, Ataliotis P, Spencer C, Sobotka A, et al. Tbx1 haploinsufficiency is linked to behavioral disorders in mice and humans: implications for 22q11 deletion syndrome. Proc Natl Acad Sci U S A. 2006;103(20):7729–34.

46. Qin Z, Wood M, Rosowski JJ. Measurement of conductive hearing loss in mice. Hear Res. 2010 May;263(1–2):93–103.

47. Bleich A, Kirsch P, Sahly H, Fahey J, Smoczek A, Hedrich H-J, et al. Klebsiella oxytoca: opportunistic infections in laboratory rodents. Lab Anim. 2008 Jul;42(3):369–75.

48. Willyard C. Squeaky clean mice could be ruining research. Nature. 2018 Apr 5;556(7699):16–8.

49. Eggermont JJ. Acquired hearing loss and brain plasticity. Hear Res. 2017 Jan;343:176–90.

50. Clarkson C, Antunes FM, Rubio ME. Conductive Hearing Loss Has Long-Lasting Structural and Molecular Effects on Presynaptic and Postsynaptic Structures of Auditory Nerve Synapses in the Cochlear Nucleus. J Neurosci. 2016 Sep 28;36(39):10214–27.

51. Sinclair JL, Fischl MJ, Alexandrova O, Heβ M, Grothe B, Leibold C, et al. Sound-Evoked Activity Influences Myelination of Brainstem Axons in the Trapezoid Body. J Neurosci. 2017 Aug 23;37(34):8239–55.

52. Xu H, Kotak VC, Sanes DH. Conductive hearing loss disrupts synaptic and spike adaptation in developing auditory cortex. J Neurosci. 2007 Aug 29;27(35):9417–26.

53. Mowery TM, Caras ML, Hassan SI, Wang DJ, Dimidschstein J, Fishell G, et al. Preserving Inhibition during Developmental Hearing Loss Rescues Auditory Learning and Perception. J Neurosci. 2019 Oct 16;39(42):8347–61.

Journal Pre-proof

54. Chun S, Du F, Westmoreland JJ, Han SB, Wang Y-D, Eddins D, et al. Thalamic miR-338-3p mediates auditory thalamocortical disruption and its late onset in models of 22q11.2 microdeletion. Nat Med. 2017;23(1):39–48.

55. Fyk-Kolodziej BE, Shimano T, Gafoor D, Mirza N, Griffith RD, Gong T-W, et al. Dopamine in the auditory brainstem and midbrain: co-localization with amino acid neurotransmitters and gene expression following cochlear trauma. Front Neuroanat. 2015 Jul 22;9:88.

56. Tong L, Altschuler RA, Holt AG. Tyrosine hydroxylase in rat auditory midbrain: distribution and changes following deafness. Hear Res. 2005 Aug;206(1–2):28–41.

57. Sohal VS, Zhang F, Yizhar O, Deisseroth K. Parvalbumin neurons and gamma rhythms enhance cortical circuit performance. Nature. 2009 Jun 4;459(7247):698–702.

58. Gothner T, Gonçalves PJ, Sahani M, Linden JF, Hildebrandt KJ. Sustained activation of PV+ interneurons in auditory cortex enables robust divisive gain control for complex and naturalistic stimuli. BioRxiv. 2019 Nov 7;

59. Martin del Campo HN, Measor KR, Razak KA. Parvalbumin immunoreactivity in the auditory cortex of a mouse model of presbycusis. Hear Res. 2012 Dec;294(1–2):31–9.

60. Brewton DH, Kokash J, Jimenez O, Pena ER, Razak KA. Age-Related Deterioration of Perineuronal Nets in the Primary Auditory Cortex of Mice. Front Aging Neurosci. 2016 Nov 8;8:270.

61. Nguyen A, Khaleel HM, Razak KA. Effects of noise-induced hearing loss on parvalbumin and perineuronal net expression in the mouse primary auditory cortex. Hear Res. 2017 Jul;350:82–90.

62. Rogalla MM, Hildebrandt KJ. Aging But Not Age-Related Hearing Loss Dominates the Decrease of Parvalbumin Immunoreactivity in the Primary Auditory Cortex of Mice. eNeuro. 2020 May 8;7(3).

63. Libé-Philippot B, Michel V, Boutet de Monvel J, Le Gal S, Dupont T, Avan P, et al. Auditory cortex interneuron development requires cadherins operating hair-cell mechanoelectrical transduction. Proc Natl Acad Sci USA. 2017 Jul 25;114(30):7765–74.

64. Meechan DW, Rutz HLH, Fralish MS, Maynard TM, Rothblat LA, LaMantia AS. Cognitive ability is associated with altered medial frontal cortical circuits in the LgDel mouse model of 22q11.2DS. Cereb Cortex. 2015 May;25(5):1143–51.

65. Al-Absi A-R, Qvist P, Okujeni S, Khan AR, Glerup S, Sanchez C, et al. Layers II/III of prefrontal cortex in df(h22q11)/+ mouse model of the 22q11.2 deletion display loss of parvalbumin interneurons and modulation of neuronal morphology and excitability. Mol Neurobiol. 2020 Aug 20;

66. Toritsuka M, Kimoto S, Muraki K, Landek-Salgado MA, Yoshida A, Yamamoto N, et al. Deficits in microRNA-mediated Cxcr4/Cxcl12 signaling in neurodevelopmental deficits in a 22q11 deletion syndrome mouse model. Proc Natl Acad Sci USA. 2013 Oct 22;110(43):17552–7.

67. Piskorowski RA, Nasrallah K, Diamantopoulou A, Mukai J, Hassan SI, Siegelbaum SA, et al. Age-Dependent Specific Changes in Area CA2 of the Hippocampus and Social Memory Deficit in a Mouse Model of the 22q11.2 Deletion Syndrome. Neuron. 2016 Jan 6;89(1):163–76.

68. Meechan DW, Tucker ES, Maynard TM, LaMantia A-S. Cxcr4 regulation of interneuron migration is disrupted in 22q11.2 deletion syndrome. Proc Natl Acad Sci USA. 2012 Nov 6;109(45):18601–6.

69. Gothner T, Gonçalves PJ, Sahani M, Linden JF, Hildebrandt KJ. Sustained activation of PV+ interneurons in core auditory cortex enables robust divisive gain control for complex and naturalistic stimuli. Cereb Cortex. 2021 Mar 31;31(5):2364–81.

Journal Pre-proof

70. Beasley CL, Zhang ZJ, Patten I, Reynolds GP. Selective deficits in prefrontal cortical GABAergic neurons in schizophrenia defined by the presence of calcium-binding proteins. Biol Psychiatry. 2002 Oct 1;52(7):708–15.

71. Hashimoto T, Volk DW, Eggan SM, Mirnics K, Pierri JN, Sun Z, et al. Gene expression deficits in a subclass of GABA neurons in the prefrontal cortex of subjects with schizophrenia. J Neurosci. 2003 Jul 16;23(15):6315–26.

72. Uhlhaas PJ, Singer W. Abnormal neural oscillations and synchrony in schizophrenia. Nat Rev Neurosci. 2010 Feb;11(2):100–13.

73. Dienel SJ, Lewis DA. Alterations in cortical interneurons and cognitive function in schizophrenia. Neurobiol Dis. 2019 Nov;131:104208.

74. Cardin JA, Carlén M, Meletis K, Knoblich U, Zhang F, Deisseroth K, et al. Driving fast-spiking cells induces gamma rhythm and controls sensory responses. Nature. 2009 Jun 4;459(7247):663–7.

75. Haenschel C, Bittner RA, Waltz J, Haertling F, Wibral M, Singer W, et al. Cortical oscillatory activity is critical for working memory as revealed by deficits in early-onset schizophrenia. J Neurosci. 2009 Jul 29;29(30):9481–9.

76. David A, Malmberg A, Lewis G, Brandt L, Allebeck P. Are there neurological and sensory risk factors for schizophrenia? Schizophr Res. 1995 Feb;14(3):247–51.

77. Fors A, Abel KM, Wicks S, Magnusson C, Dalman C. Hearing and speech impairment at age 4 and risk of later non-affective psychosis. Psychol Med. 2013 Oct;43(10):2067–76.

78. Mason P, Rimmer M, Richman A, Garg G, Johnson J, Mottram PG. Middle-ear disease and schizophrenia: case-control study. Br J Psychiatry. 2008 Sep;193(3):192–6.

79. Hayashida Y, Mitani Y, Hosomi H, Amemiya M, Mifune K, Tomita S. Auditory brain stem responses in relation to the clinical symptoms of schizophrenia. Biol Psychiatry. 1986 Feb;21(2):177–88.

80. Källstrand J, Nehlstedt SF, Sköld ML, Nielzén S. Lateral asymmetry and reduced forward masking effect in early brainstem auditory evoked responses in schizophrenia. Psychiatry Res. 2012 Apr 30;196(2–3):188–93.

81. Lindstrom L, Klockhoff I, Svedberg A, Bergstrom K. Abnormal auditory brain-stem responses in hallucinating schizophrenic patients. Br J Psychiatry. 1987 Jul;151:9–14.

82. Zinnamon FA, Harrison FG, Wenas SS, Meyer AF, Liu Q, Wang KH, et al. Hearing loss promotes schizophrenia-relevant brain and behavioral abnormalities in a mouse model of human 22q11.2 Deletion Syndrome. BioRxiv. 2019 Feb 3.

Journal Pre-proof

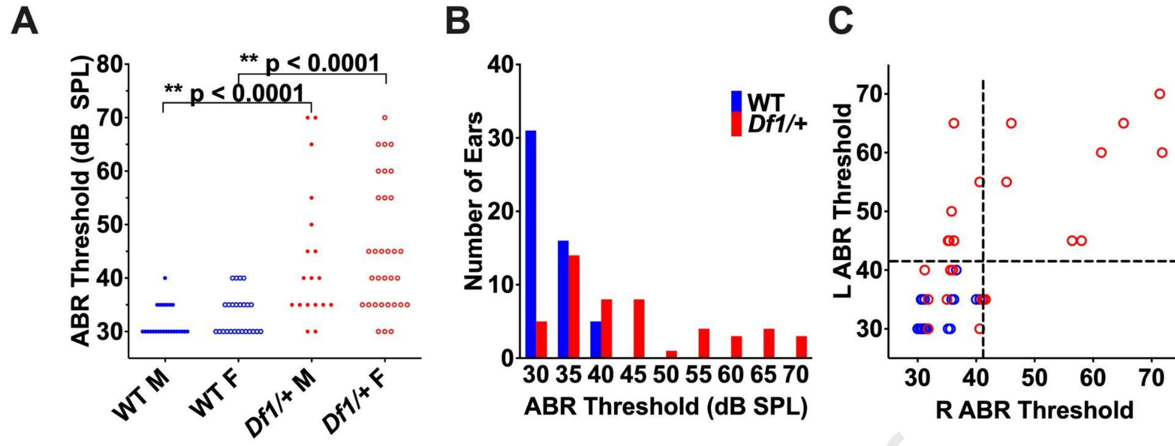

Journal Pre-proof

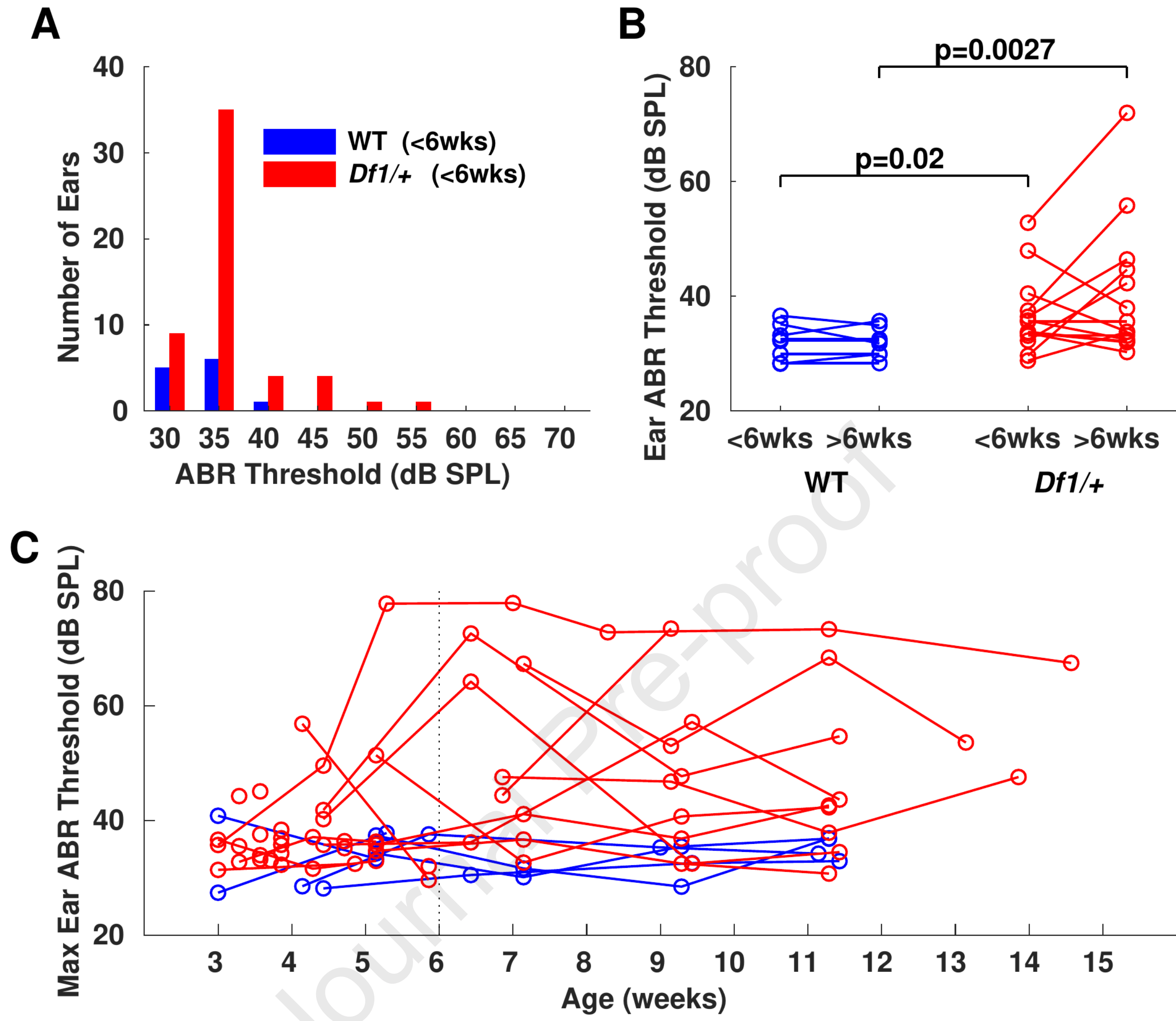

Journal Pre-proof

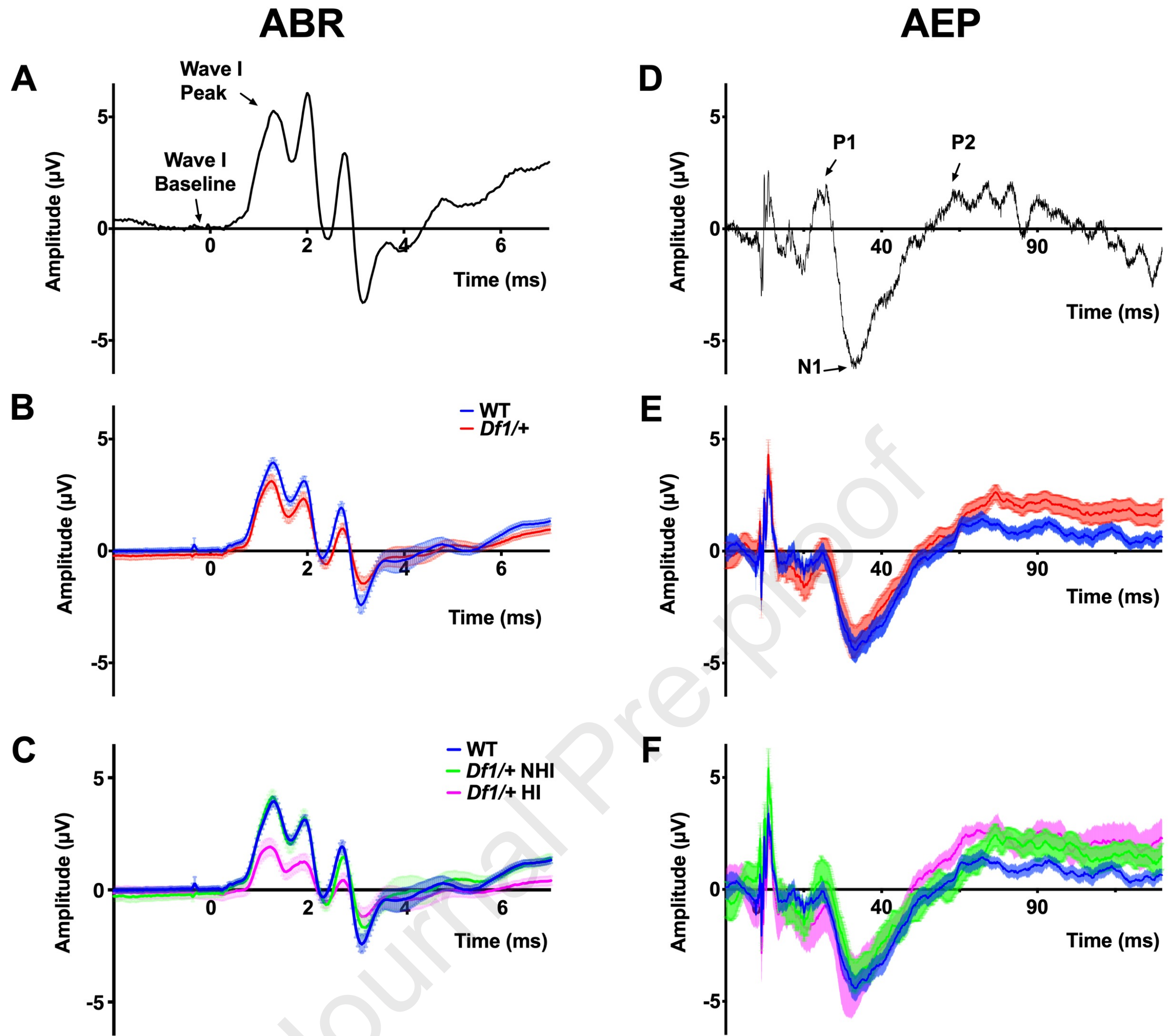

Journal Pre-proof

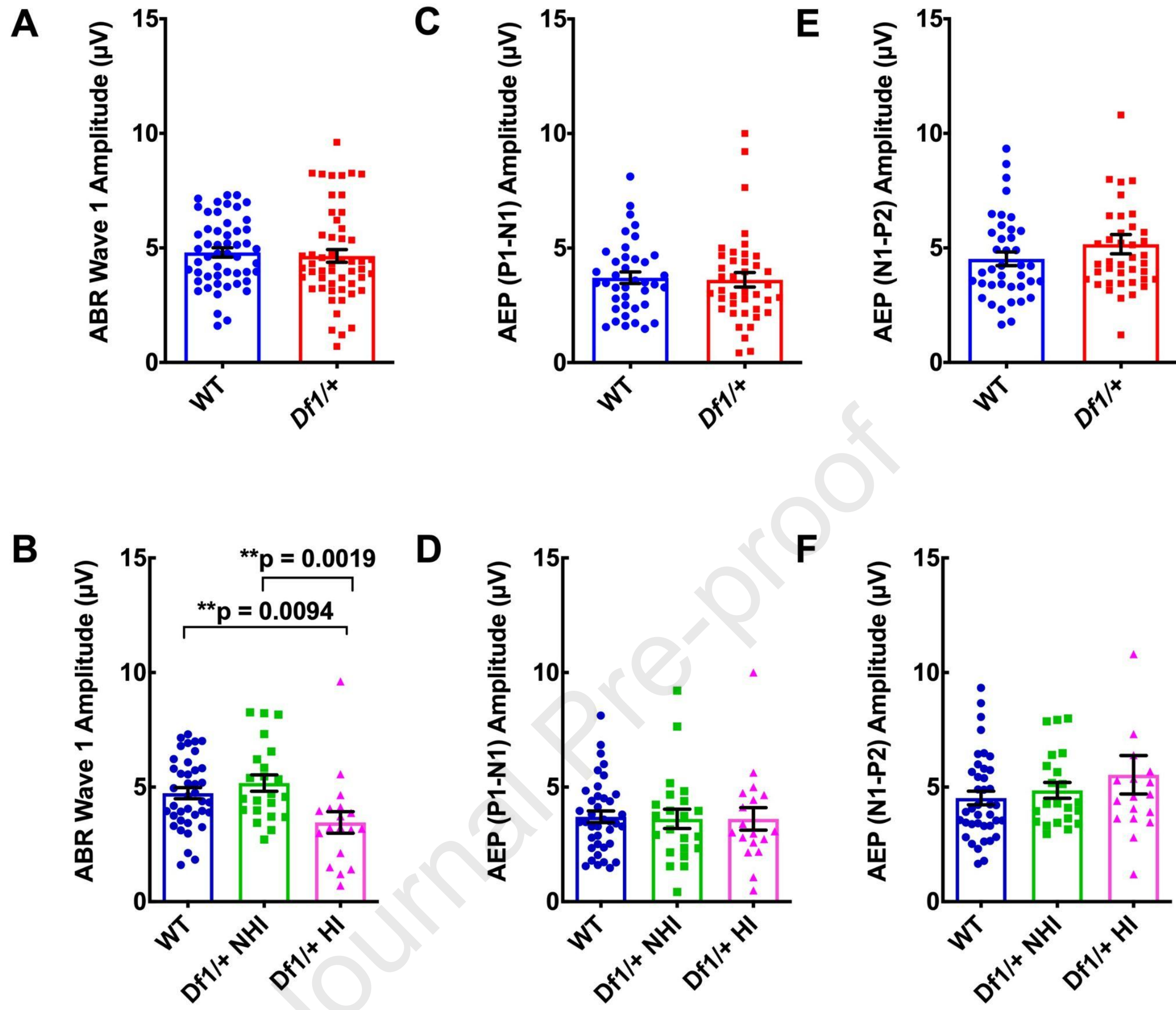

Journal Pre-proof

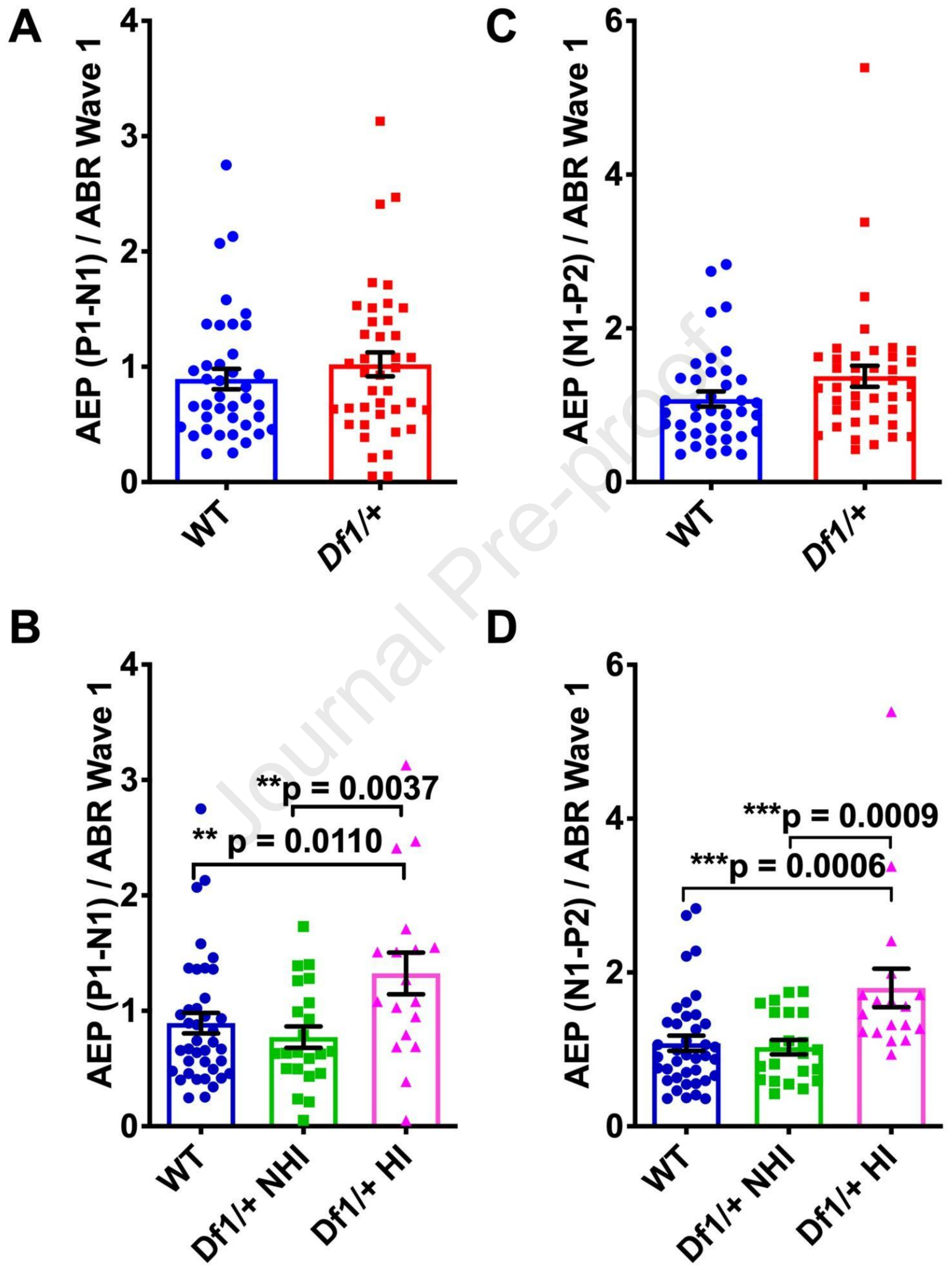

Journal Pre-proof

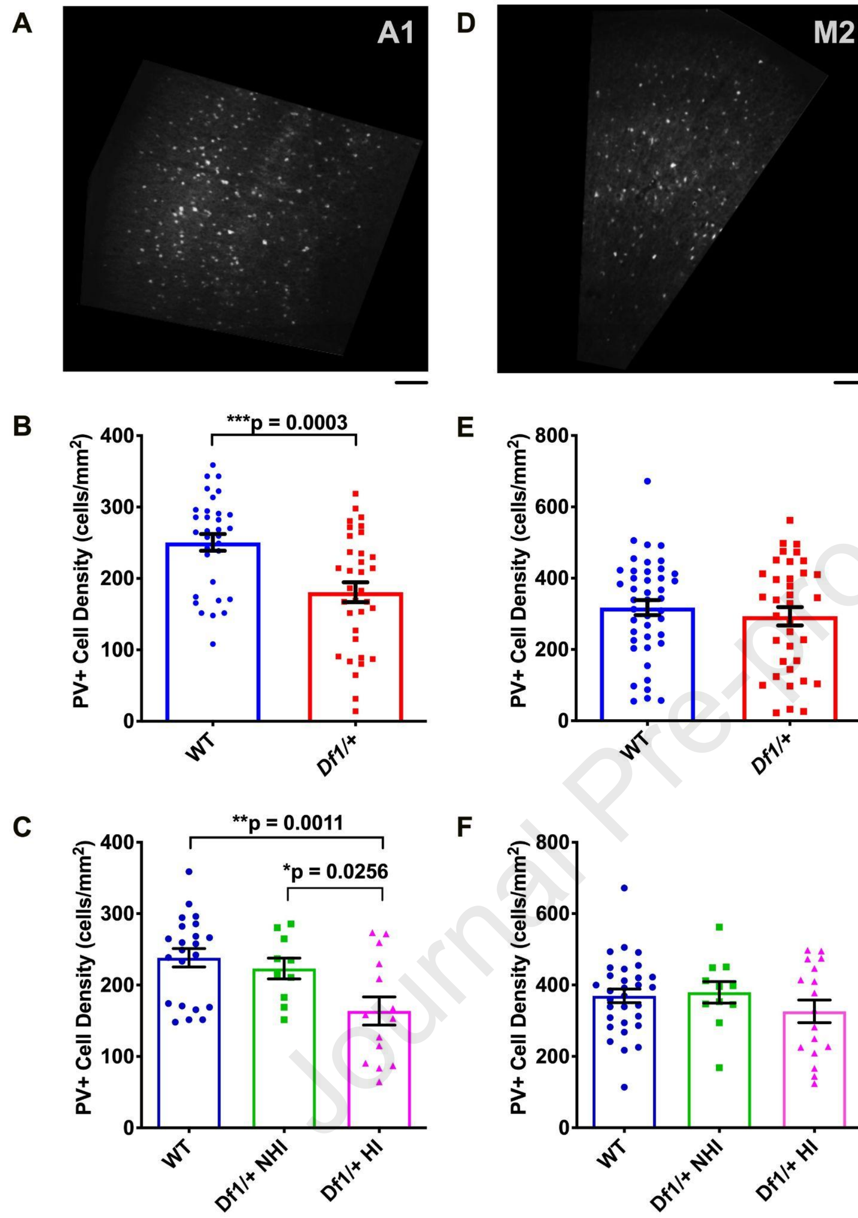

Journal Pre-proof

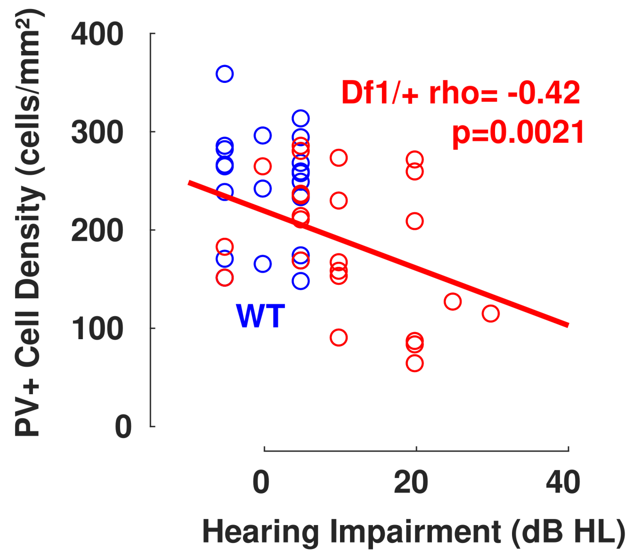

Journal Pre-proof